

Projections of land cover change and its implications for water yield in the Maros watershed

Faisal Hidayat^{1*}, Andang Suryana Soma², Mahmud Achmad³,
Muhammad Dandy Rachmat Ramadhan², Nurjannah Oktorina Abdullah⁴

¹ Master Program of Regional Planning and Development, Hasanuddin University, 90245, Makassar, Indonesia

² Faculty of Forestry, Hasanuddin University, 90245, Makassar, Indonesia

³ Department of Agricultural Technology, Faculty of Agriculture, Hasanuddin University, 90245, Makassar, Indonesia

⁴ Environmental Science Study Program, Faculty of Mathematics and Natural Sciences, Universitas Negeri Makassar, 90224, Indonesia

* Corresponding author's e-mail: hidayatf23p@student.unhas.ac.id

ABSTRACT

The decline in water yield in the Maros watershed, which is located in the Mamminasata national strategic area, is influenced by land cover changes that occur in response to development in the watershed. The aims of this study are (1) to project future land cover changes (2032) via the CA-ANN approach and (2) to analyze the effects of these land cover changes on water yield via the SWAT model. In the SWAT simulation, the land cover map of 2023 and the projection map of 2032 were used as scenarios. SWAT-CUP was also used to validate the SWAT model. River Batubassi and River Lekopancing had R2 values of 0.7257 and 0.7802, respectively, indicating that the model worked well. The land cover change projections showed a decrease of 208.55 hectares of secondary forest and a decrease of 104.99 hectares of secondary mangrove forest, respectively. Additionally, the areas of settlements, fish ponds, paddy fields, and agriculture/crop land increased by 87.19 hectares, 95.79 hectares, 86.59 hectares, and 94.38 hectares, respectively. The SWAT simulation revealed that the water yield decreased from 31.09 billion m³ in 2023 to 21.65 billion m³ in 2032. A decrease in annual rainfall and a decrease in vegetated land area triggered a decrease in water yield.

Keywords: Maros watershed, land cover change, 2032 projection, water yield, SWAT, MOLUSCE, CA-ANN.

INTRODUCTION

The amount of water flowing in a watershed from surface flow, lateral flow, and groundwater flow after water losses such as evaporation and water use by vegetation are subtracted is defined as the water yield (Neitsch et al., 2011). Water yield determines water availability in a watershed and is affected by land cover because land cover affects hydrological processes, including infiltration, evapotranspiration, and surface lateral processes (Tian et al., 2022). Vegetated land cover, such as forests, has the ability to support increased infiltration and longer water storage, thereby supporting sustainable water availability

(Truong et al., 2022). Conversely, nonvegetation or degraded land cover tends to support increased surface runoff and a decrease in the watershed's ability to maintain water yield (Thakur et al., 2017) (Ridwansyah et al., 2018).

In the Mamminasata (Makassar, Maros, Sungguminasa, and Takalar) national strategic area, the Maros watershed plays an essential role in driving regional growth. This watershed is expected to support regional development activities, especially in providing a sufficient water supply. However, this watershed faces ecological problems in the form of land cover changes from vegetation to nonvegetation. Historical data show that deforestation of 1,105.72 hectares occurred

in this watershed between 1990 and 2020, as listed in Table 1 (Badwi et al., 2023).

Another problem that occurs in the Maros watershed is the intensification of agriculture, which does not consider the conservation of soil and water. This triggers the erosion of soil, which in turn leads to the occurrence of critical land at a rate of 372.94 hectares/year (Imran and Djafar, 2020). In addition, the urbanization that has occurred in the Maros watershed has also pressured the quality and quantity of water resources. The increase in the area of settlements in this watershed has increased the peak discharge of the river by 6–10 times compared with previous conditions and has caused a decrease in water quality, especially the BOD parameter (Syafri et al., 2020). In general, land cover changes from vegetation to non-vegetation disrupt the hydrological conditions of watersheds, which in turn can cause problems such as drought during the dry season and flooding during the rainy season. (Pahar et al., 2021).

Several studies related to land cover changes that have been conducted in the Maros Watershed, namely research conducted by (Latief et al., 2021) which looked at the effect of land cover changes on flooding in the Maros Watershed using the overlay mapping method and simple linear regression; (Nurhidayat, 2022) who looked at the effect of land cover changes on peak river discharge in the Tanralili sub-watershed (one of the sub-watersheds in the Maros Watershed) using the hydrograph method; (Sari, 2022) who looked at the level of erosion using the SWAT model in the Tanralili Sub-watershed (one of the sub-watersheds in the Maros Watershed), these study did not use predictive spatial modeling to predict future land cover changes in the Maros Watershed and did not discuss future water yields under changing land cover conditions. (Barkey and Nursaputra,

2019) conducted research who used SWAT to assess changes in forest conditions and their impact on water availability, but this study has not predicted future water availability with future land cover change scenarios; (Nurmiaty and Baja, 2013) who analyzed future land cover changes in the Maros Watershed using Cellular Automata and Markov Chain, but this study did not discuss the impact of future land cover changes on water yields. Research that has been conducted in the Maros Watershed still focuses on the impact of land cover changes on hydrological processes, flooding, erosion, and water availability using historical or current data but has not used projections of future land cover changes. This is what prompted us to conduct research to model future land cover changes and how they will affect future water quantities in the Maros watershed.

In order to address these gaps, predictive tools such as the Cellular Automata-Artificial Neural Network (CA-ANN) model can be used for predicting land cover changes. It can simulate spatial patterns of future land cover changes using historical data on previous land cover changes and the factors that influence those changes (Lukas et al., 2023). Similarly, the Soil and Water Assesment Tool (SWAT) model can be used to examine the impact of land cover change on water yield. Several studies have demonstrated that the model can simulate processes of hydrology in watersheds both spatially and temporally, as demonstrated in South Africa (Smit et al., 2024), Canada (Islam et al., 2024), and Indonesia (Wiwoho et al., 2021). As a hydrological model, SWAT can also function effectively, as demonstrated by the validation of the SWAT model, which shows good performance as seen through the statistical parameter of the coefficient of determination (R²) (Wiwoho et al., 2021).

Table 1. Forest conversion in the Maros Watershed, 1990–2020

Initial land cover	Final land cover	Area (Ha)
Forest	Former Logging Area	19.34
Forest	Scrubland	129.13
Forest	Settlements/Built-up Areas	28.93
Forest	Savannah/Grassland	31.10
Forest	Water Bodies	0.40
Forest	Mixed Gardens	609.32
Forest	Rice Fields	239.68
Forest	Open Land	47.82
Total		1,105.72

On the basis of this background, the aims of this study are (1) to project future land cover changes in the Maros watershed via the CA-ANN model approach and (2) to analyze the effects of land cover changes on water yield via the SWAT model. By identifying specific relationships between predicted land cover transitions and water yield under the influence of climatic conditions, this study aims to make a scientific contribution. We hypothesize that, couple with declining rainfall, the ongoing conversion of vegetated land cover to non-vegetated land cover will significantly reduce water production and increase the risk of water scarcity in the Maros watershed.

MATERIALS AND METHODS

Research location

This study was conducted in the Maros watershed, which is part of the Mamminasata national strategic area. Administratively, the Maros watershed, which covers an area of 72348.95 hectares, encompasses four districts/cities in South Sulawesi Province. Maros Regency covers nearly 92% of the watershed area, whereas Gowa Regency, Bone Regency, and Makassar city cover the remainder of the watershed area. Table 2 shows the area of the Maros watershed based on administrative regions.

Geographically, the Maros watershed is located at coordinates 119°55'45.79" – 119°27'56.85" East Longitude and 5°8'3.45" – 5°1'33.45" South Latitude. The existence of this watershed is essential for supporting the development of the Mamminasata region because it is expected to provide water resources for development, including domestic, agricultural, and industrial needs.

Owing to its topography, the Maros watershed has various landforms because it is located in a transition zone between mountainous and lowland areas. These conditions affect land cover patterns and hydrological conditions in the Maros watershed. The average annual rainfall in this

region reaches 2408.00 mm. This indicates that the climate in this region has high rainfall (Endarwin et al., 2013).

Based on soil classification up to the Great Group level, the Maros watershed has 12 soil type combinations, as shown in Figure 1. This indicates that the level of soil diversity in this watershed is quite high. The most dominant soil groups in this watershed are the Tropaquepst, Fluvaquents, and Ustropepts groups, which cover 30.25% of the watershed area. This level of soil diversity reflects the complex physical characteristics of the watershed, which affect the processes of hydrology in the Maros watershed. Figure 2 shows the location where this research was conducted.

Analysis of projected land cover change

To assess the hydrological impacts of land cover change in the Maros Watershed (DAS), we first conducted a comprehensive analysis of the projected land cover change. Next, we evaluated current and future water production because land cover change significantly affects hydrological processes such as infiltration, evapotranspiration, and surface runoff. All of these processes collectively affect water production (Dutra et al., 2022). We used the Cellular Automata-Artificial Neural Network (CA-ANN) model integrated in the MOLUSCE plugin in QGIS to simulate the spatial pattern of land cover transition using historical land cover data and drivers of change. This provides a reliable framework for predicting future land use scenarios (Muhammad et al., 2022). The following steps illustrate the systematic approach taken to analyze projected land cover changes.

Land cover data collection and processing

For this study, land cover maps from 2014, 2019, and 2023 were used as the foundation for this analysis. These three maps were produced through image interpretation and classification. The 2014, 2019, and 2023 images were downloaded from Landsat 8 OLI satellite imagery on June 25, 2024

Table 2. Area of the Maros watershed based on administrative regions

No	Regency/City	Area (ha)	Percentage (%)
1	Maros	66,400.84	91.779
2	Gowa	5,941.44	8.212
3	Bone	4.64	0.006
4	Makassar	2.04	0.003

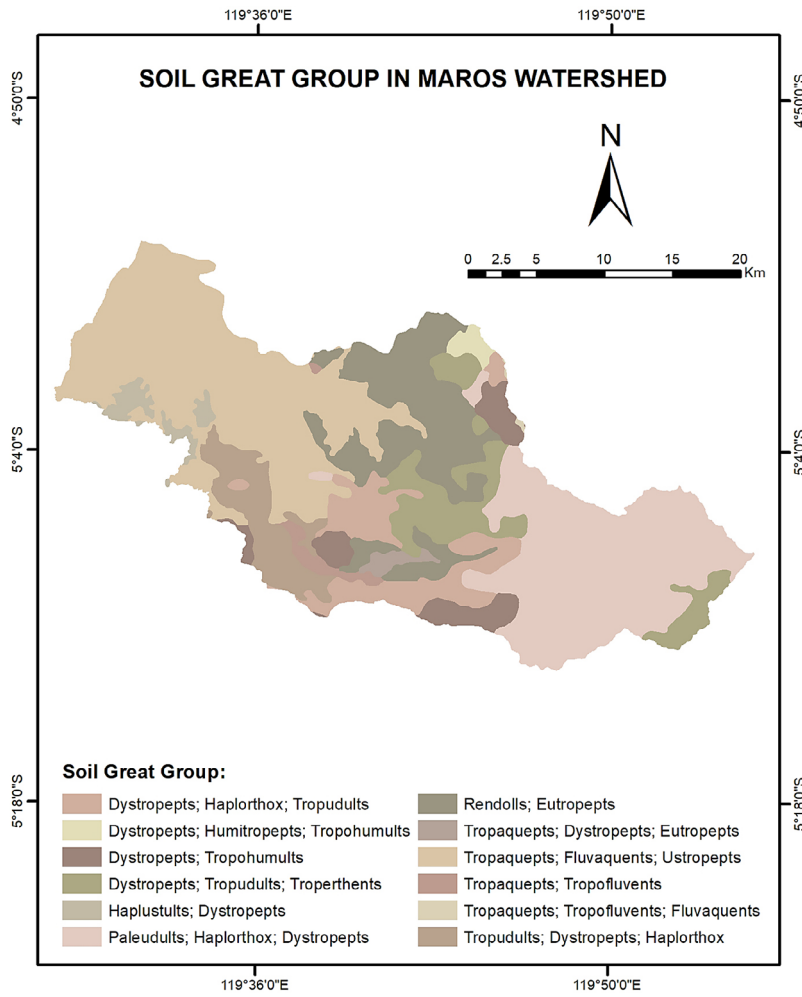


Figure 1. Soil great group in the Maros watershed

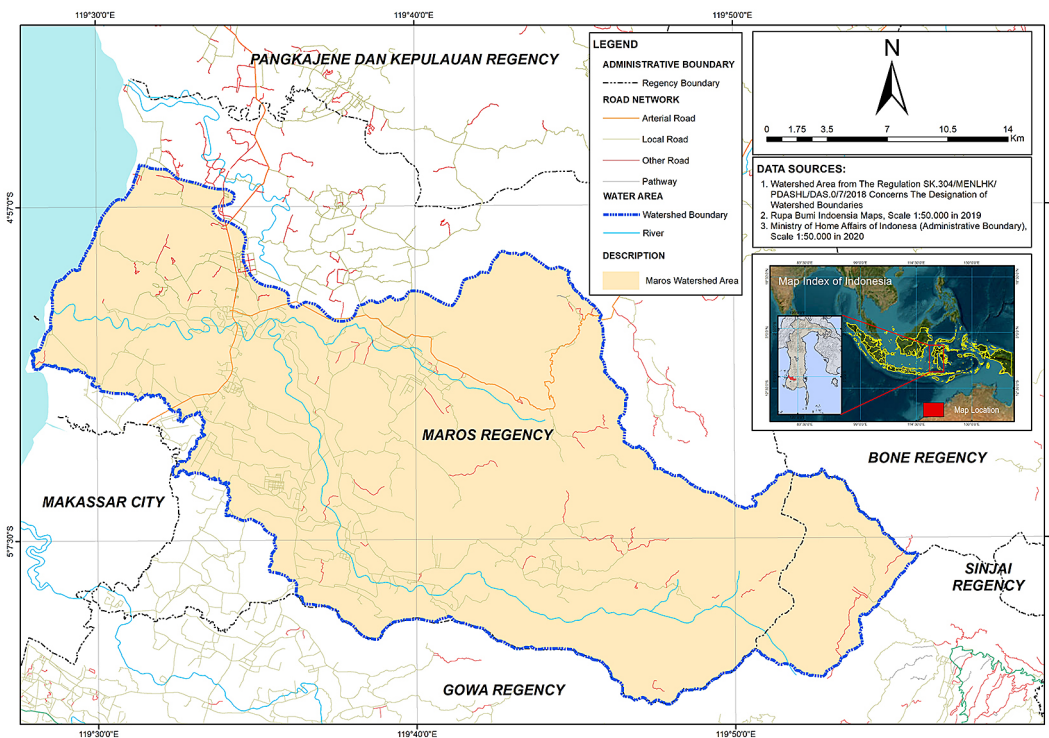


Figure 2. Research location

via <https://earthexplorer.usgs.gov/>. A false color composite was then created by combining band 6 (SWIR1), band 5 (NIR), and band 4 (Red) for land cover classification. This band combination enables clearer differentiation between objects on the Earth's surface, as it provides better contrast between objects such as vegetation, settlements, and water bodies compared to their natural color appearance. The images were then classified via guidelines based on the technical guidelines issued by the Indonesian Ministry of Environment and Forestry. The classification results were then validated via a confusion matrix with overall accuracy and kappa coefficient indicators. These three maps were then converted to raster format with a 30-meter resolution for further analysis in Molusce.

Identification and preparation of land change drivers

To model land cover changes, six main factors were identified based on their influence on land use dynamics in the DAS: elevation, slope, distance from roads, distance from rivers, distance from forest, and distance from settlements. These factors describe the spatial relationship between land cover transitions and environmental and anthropogenic factors (Abbas et al., 2021). Elevation and slope data were taken from a digital elevation model (DEM) with a resolution of 30 meters. Distance-based factors namely distance from roads, rivers, forests, and settlements were calculated using the Euclidean distance function in QGIS, based on vector data for roads, rivers, forest boundaries, and settlement locations sourced from regional topographic maps and land use plans. All driver datasets were converted to a 30-meter resolution raster format, aligned with the land cover map, and normalized to enable compatibility with the CA-ANN model. This preprocessing step enabled that the drivers accurately represent the spatial pressures affecting land cover change.

Land cover change modeling in MOLUSCE

The CA-ANN model was trained and verified with the MOLUSCE plugin in QGIS to simulate land cover changes. As a basis for model training, land cover change modeling was conducted by inputting the land cover map for 2014 as the initial map, the land cover map for 2019 as the final map, and the drivers of land cover change. Subsequently, ANN model training was conducted to construct the 2014-2019 land cover change

model. The Artificial Neural Network (ANN) was trained for 1,000 iterations with a learning rate of 0.01 and a momentum of 0.9 to establish the spatial-statistical relationship between land cover change and its driving factors. The ANN model describes the spatial-statistical relationship between the land change that occurred and the land change drivers used. After the ANN model was formed, it was simulated via the CA approach until 2023, resulting in a simulated 2023 land cover map. The CA approach simulates land cell changes by considering the conditions of neighboring cells (Amgoth et al., 2023). To evaluate the suitability level, the simulated land cover map of 2023 was compared with the land cover map of 2023, which was generated from image interpretation. For the model to be used in subsequent analyses, it was verified via the kappa coefficient, a statistical measure that compares the predicted results with the actual reference data (Anggari et al., 2023). The validated CA-ANN model is then utilized to project future land cover changes (by 2032). Assumes continuation in observed driving factors and transition trends.

SWAT model analysis (soil and water assessment tool)

The analysis of available water in the Maros watershed was conducted utilizing the SWAT hydrological model approach because water yield is one of the outputs produced by the SWAT model. SWAT is one of the hydrological models that can be utilized to check the effects of interactions between land cover, slope, soil characteristics, and climate on water flow, water quality, erosion, and sedimentation in a watershed (Smit et al., 2024). Water yield in SWAT is defined as the total volume of water available on the surface and flowing toward the watershed outlet, which is the accumulation of surface flow, lateral flow, and base-flow minus water loss and abstraction from ponds and reservoirs (Neitsch et al., 2011). The equation used to calculate water yield is as follows:

$$WYLD = Q_{surf} + Q_{lat} + Q_{gw} - \text{tloss} - \text{pond abstractions} \quad (1)$$

where: Q_{surf} – surface flow (mm), Q_{lat} – lateral flow (mm), Q_{gw} – ground flow (mm), $tloss$ – water loss to the aquifer (mm), $pond\ abstraction$ – the amount of water lost due to artificial water storage such as ponds or reservoirs.

Data and modeling stages

To run SWAT, four data are used:

- DEM (digital elevation model) data – this study used the 30 m resolution ASTER DEM, which was downloaded on October 30, 2024. DEM is a digital representation of the Earth's surface elevation in raster or grid form. DEM data in the SWAT model is stored in raster format and UTM projection. Before using DEM as SWAT input, a basin filling process must be carried out to prevent discontinuities. DEM is used to form river networks, determine watershed boundaries, and calculate topographic parameters such as flow direction, slope gradient, and slope length (Tran et al., 2023).
- land cover data – this study uses the 2023 land cover map and the 2032 land cover projection. The 2023 land cover map was retrieved through image interpretation and classification, and the 2032 land cover projection map was retrieved through the CA-ANN approach based on previous land cover change data via Mollusca. In SWAT, the land cover map was created via raster format and UTM projection. Before the land cover map is used as the SWAT input, the land cover class names owned by the SWAT must be adjusted.
- soil data – the soil data used was obtained from a 1:250,000 scale Repprot landsystem map. The data was then detailed through soil sampling in the field based on the formed land units (Busico et al., 2020). To determine the physical and chemical properties of the soil that influence the process of hydrology, the soil data was tested in a laboratory. The following are the physical and chemical soil properties used in this study: soil crack volume (SOL_CRK); available water capacity (SOL_AWC); saturated hydraulic conductivity (SOL_K); soil albedo (SOL_ALB); texture (TEXTURE); soil depth (SOL_Z); bulk density (SOL_BD); permeability (SOL_KSat); organic carbon content (SOL_CBN); clay percentage (CLAY); silt percentage (SILT); sand percentage (SAND); soil erodibility (USEL_K); pH (SOL_PH). The soil map used as input for SWAT uses a raster format and UTM projection. The soil data to be used as input for SWAT must be adjusted to the SWAT format.
- climate data – the climate data used come from NASA's MERRA-II satellite. The data include precipitation, maximum and minimum

temperatures, humidity, wind speed and solar radiation (Aznarez et al., 2021). Through the website <https://power.larc.nasa.gov/>, the data were downloaded on October 30, 2024. Before the climate data are downloaded, we need to determine the climate station that represents the climate conditions in the Maros watershed area. Here, the CSIRO model climate station is used.

The model is run via a SWAT extension in ArcGIS called ArcSWAT with the following stages:

- a) delineation of the watershed boundary – the first step is delineation, which means that the watershed is divided into smaller units called subwatersheds. Through the watershed delineation module, this process is carried out automatically via DEM data, which are used to determine the direction of water flow, the river network, watershed outlets, and the division of subwatersheds (Femeena et al., 2022). Technically, the delineation process is carried out through four stages: (1) inputting DEM data into ArcSWAT; SWAT calculates the slope and fill depressions; (2) determining the flow direction and accumulation; the system automatically calculates the flow direction and accumulation; (3) determining watershed outlets; here, the system creates watershed outlets via the automatic watershed outlet selection module; and (4) defining the river network: the system creates a river network on the basis of the threshold area; the larger the threshold area value is, the fewer river networks and subwatersheds will be formed. (5) Delineation results: Here, we can see the results of the delineation process, which consists of watershed boundaries, subwatersheds, river networks, and outlet points.
- b) formation of the HRU (hydrologic response unit) – after the subwatershed is formed, the subwatershed is then divided into smaller units called HRUs. A combination of land cover, soil type, and slope class is called an HRU. HRU is considered hydrologically homogeneous. This HRU is the basis for calculating physical processes such as the surface flow rate, infiltration, erosion and sedimentation, evapotranspiration, and nutrient transport (Zare et al., 2022). Technically, the HRU formation process is carried out through stages (1) by entering a map of land cover, a map of the soil type, and a map of the slope class in the HRU analysis menu in ArcSWAT; (2) by reclassifying and setting up data, at this stage, the land classification code

that we have is connected to the SWAT code, the SWAT soil database is used, and the slope class interval is determined; (4) by overlaying a map of land cover, a map of the soil type, and a map of the slope class, here, we need to determine the threshold to remove very small combinations; and (5) by forming HRUs via the create HRU menu, the SWAT model generates a list of HRUs in each subwatershed, an attribute table related to HRUs.

- c) climate data processing – climate data are important data in hydrological process simulations because these climate data affect processes of hydrology, namely, evapotranspiration, surface flow, infiltration, soil moisture, and runoff (Dahal et al., 2020). Technically, climate data processing is carried out through the following stages: (1) Climate data are collected; here, we download climate data from the official USGS website. There are 6 climate parameters that we downloaded, namely, precipitation, maximum temperature, minimum temperature, humidity, wind speed, and solar radiation. (2) Compile master data for each climate parameter with the formats pcp.txt, tmp.txt, hmd.txt, wnd.txt, and slr.txt according to station (3), and enter the climate data into ArcSWAT via the weather data definition menu.
- d) SWAT model simulation – SWAT simulation is carried out after the process of delineating subwatershed boundaries, forming HRUs, and processing climate data is carried out. Through SWAT simulation, we can calculate water balance components such as surface flow, base flow, sedimentation, and evapotranspiration. Technically, the SWAT simulation process is carried out through stages (1) setting up the project and entering the input; here, we must ensure that the watershed delineation has been carried out, the HRU has been formed, and daily climate data have been installed. Next, we enter the SWAT simulation module and select the edit SWAT input (2) set the simulation parameters in the SWAT simulation setup menu. At this stage, we can set the simulation period parameter for the time range, select daily/monthly/annual time steps, use daily data for weather input, and select daily/monthly/annually internal outputs. (3) Run the simulation; here, we select the write input table menu and then select the Run SWAT simulation menu. (4) See the simulation results; here, we can open the SWAT output menu and determine the SWAT output. In this study, we

simulated two land cover scenarios to determine the impact of land cover changes on the water yield in the Maros watershed. We do this via the 2023 land cover map and the 2032 projected land cover map.

RESULTS AND DISCUSSION

Land cover classification

On June 25, 2024, Landsat 8 Operational Land Imager (OLI) satellite imagery was obtained from the USGS EarthExplorer platform (<https://earthexplorer.usgs.gov/>) and used for the interpretation and classification of land cover maps for 2014, 2019, and 2023. False color composition (Bands 6-SWIR1, 5-NIR, 4-Red) was used to clearly differentiate 13 land cover classes: airport area, secondary forest, secondary mangrove forest, plantation forest, settlement, agricultural land/food crops, mixed agriculture/agroforestry, grassland, rice field area, shrubland, fish pond, open area, and water. The Indonesian Ministry of Environment and Forestry guidelines were used as the basis for classification, with training samples obtained from field surveys and high-resolution imagery. High accuracy was achieved through confusion matrix validation. The overall coefficient and kappa are 0.99 and 0.98 (2014), 0.99 and 0.98 (2019), and 0.98 and 0.97 (2023), indicating a “very good” classification value because the kappa is above 0.80 (Anggari et al., 2023). This metric indicates that the land cover map is reliable for further modeling. Figure 3 shows the spatial distribution of land cover classes for 2014, 2019, 2023, and the 2032 projection map. Showing transitions such as forest loss and settlement expansion.

Modeling of land cover change

To predict land cover change until 2032, the CA-ANN model was used with the MOLUSCE plugin in QGIS. The model was trained using the 2014 land cover map (initial state) and the 2019 map (final state), as well as six driving factors: slope, elevation, distance from roads, rivers, forest area, and settlements. The impact of driving factors on land cover change from 2014 to 2019 was measured by Pearson correlation analysis, which can be seen in Table 3.

From Table 3, it is known that the distance from roads ($r = 0.681$ with settlements) and the

Table 3. Coefficient of Pearson correlation for drivers of land cover change (2014–2019)

Driving factors	Elevation	Distance from forest area	Distance from settlement	Distance from river	Distance from road	Slope
Elevation	--	-0.411	0.511	-0.249	0.547	0.550
Distance from forest area		--	-0.445	0.553	-0.380	-0.480
Distance from settlement			--	-0.218	0.681	0.466
Distance from river				--	-0.197	-0.319
Distance from road					--	0.441
Slope						--

distance from settlements ($r = 0.511$ with elevation) are the most significant factors in the analysis, showing the impact of urbanization and accessibility on land cover change. In order to replicate spatial changes, an artificial neural network (ANN) was configured with two hidden layers (each consisting of 100 neurons), trained for 1,000 iterations (learning rate 0.01, momentum 0.9), and connected to a CA. Simulated land cover maps for 2023 and actual maps for 2023 were compared to validate the model. The model’s kappa coefficient of 0.85 shows “very good” accuracy (Anggari et al., 2023). Through three five-year cycles, the verified model was used to predict land cover up to 2032.

Projections of land cover in 2032

The result of land cover projections for 2032 show significant shifts in land cover, driven by anthropogenic pressures. Table 4 assesses changes

between 2023 and 2032, showing a reduction in natural vegetation cover and an expansion in developed land use. From Table 4, it is known that the tendency of land utilized for anthropogenic purposes has increased, especially for the purposes of settlements (+87.19 hectares, +2.29%), fish ponds (+95.79 hectares, +1.67%), and paddy area (+86.59 hectares, 0.62%). Moreover, natural land cover shows a notable decline such as in secondary forests (-208.55 hectares, 0.83%) and secondary mangroves forest (-104.99 hectares, 36.79%). This change shows that development increases pressure on the natural ecosystems of the watershed, and has the potential to increase surface runoff and soil infiltration capacity and reduce groundwater availability. As a result, the water supply between the rainy and dry seasons is increasingly imbalanced, increasing the risk of drought. Figure 3 illustrates this transition, showing the spatial contraction of forest areas and the expansion of settlements along the road network.

Table 4. Land cover changes 2023–2032

No	Land cover	Area (ha)		Change	
		2023	2032	Area (ha)	%
1	Airport area	380.12	382.79	-2.67	0.70
2	Secondary forest	25,223.95	25,015.40	-208.55	0.83
3	Secondary mangrove forest	285.59	180.6	-104.99	36.76
4	Planted forest	1,985.24	2,011.00	25.76	1.30
5	Settlement	3,811.65	3,898.84	87.19	2.29
6	Agricultural/crop land	9,595.94	9,690.32	94.38	0.98
7	Mixed agricultural/agroforestry	8,179.10	8,147.61	-31.49	0.39
8	Grassland	529.15	461.62	-67.53	12.76
9	Paddy area	14,007.22	14,093.81	86.59	0.62
10	Shrubland	1,321.55	1,317.02	-4.53	0.34
11	Fish pond	5,723.20	5,818.99	95.79	1.67
12	Open area	539.43	526.04	-13.39	2.48
13	Water	766.81	804.91	38.1	4.97
Luas total DAS		72,348.95	72,348.95		

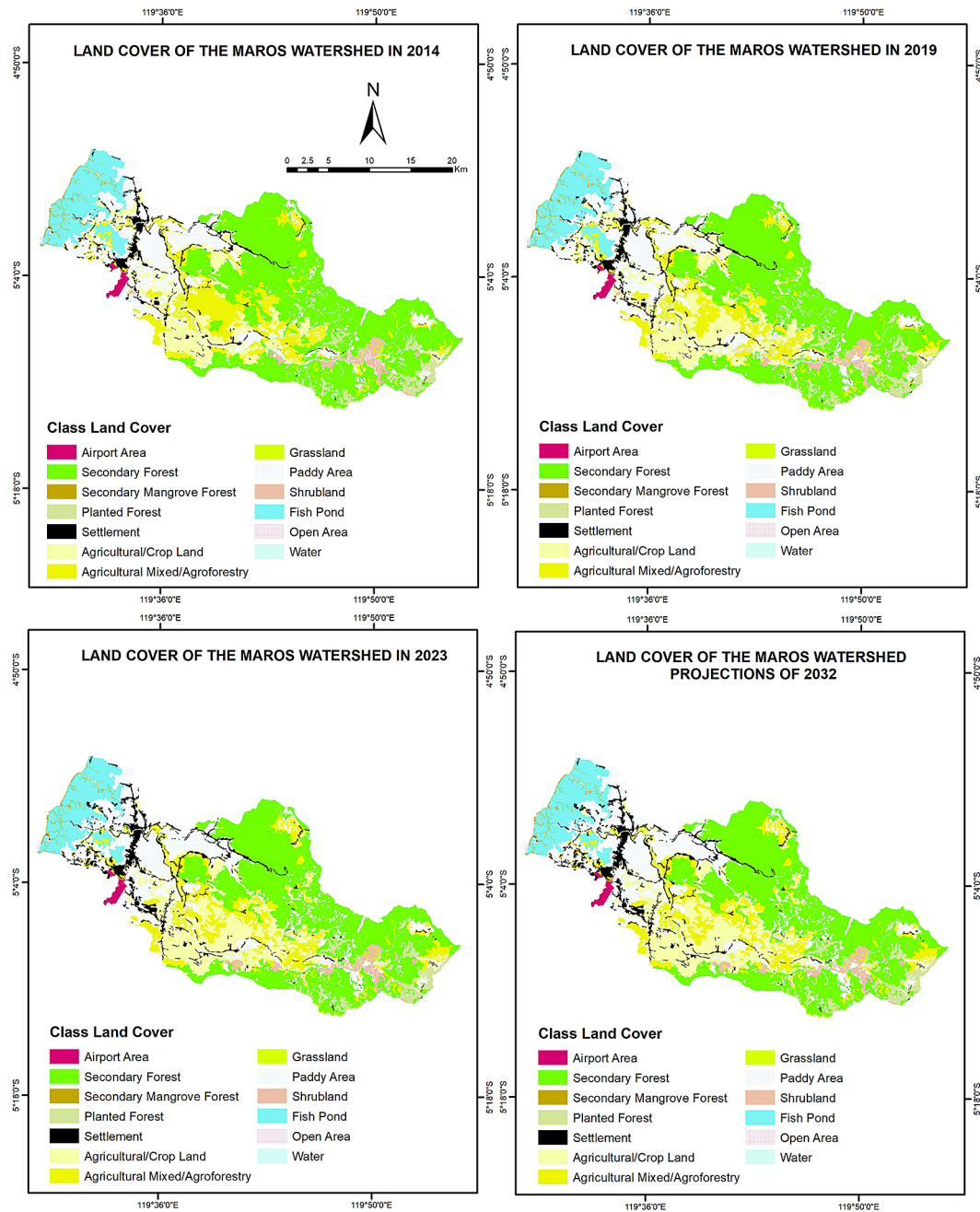


Figure 3. Land cover maps for 2014, 2019, 2023, and 2032

Results of SWAT model analysis in the Maros watershed

Delineation of subwatershed boundaries

DEM data with a resolution of 30 m was used to delineate the watershed. In this study, the delineation process conducted in ArcSWAT, generated 48 subwatersheds with a minimum threshold area of 10 hectares to ensure that the entire river network in the Maros watershed is represented in the model. Subwatershed with the largest area is subwatershed 22 reaching 3,822.95 hectares

(about 5.28% of the total watershed area). While the subwatershed with the smallest area is subwatershed 28 covering 3.44 hectares (about 0.005% of the total watershed area). The Multiple Slope Classification method is also used to automatically create the slope class map using DEM data. Slope classes were categorized as 0–8% flat; 8–15% gentle; 15–25% slightly steep; 25–45% steep; > 45% very steep (Amin et al., 2021). Figure 4 illustrates the distribution of slope class, showing topographic variability affecting hydrological processes.

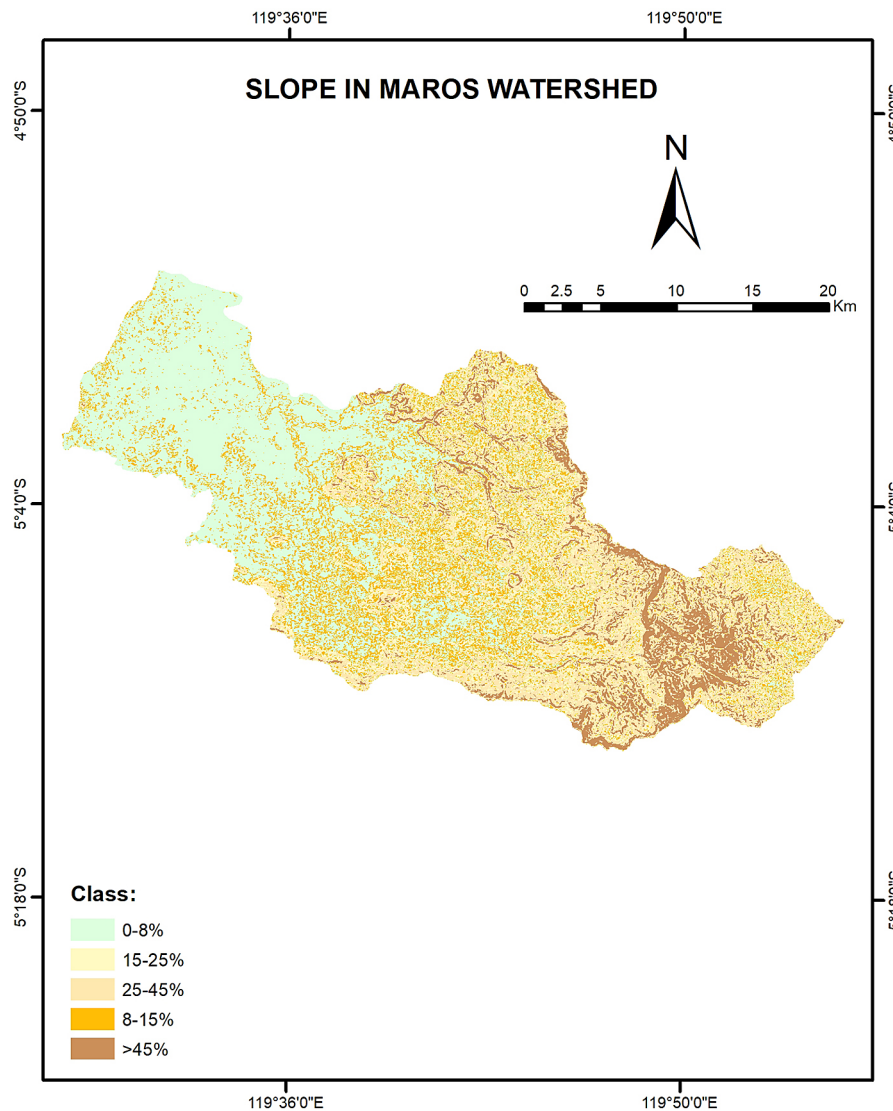


Figure 4. Slope class map of Maros watershed

Establishment of the HRU

Slope maps, soil type maps (derived from regional soil surveys), and land cover maps from 2023 and 2032 are combined to establish HRUs. The “Edit SWAT Input” component of the SWAT database was used to enter physical and chemical characteristics of the soil, such as texture and hydraulic conductivity. To facilitate geographically detailed hydrological simulations, this method generated 3.278 HRUs, each representing a unique combination of land cover, soil type, and slope characteristics.

Climate data processing

Climate data for the last ten years (2014–2023) were downloaded from NASA’s POWER [ascendancy=1” href=](https://power.nasa.gov/)

[data-access-viewer/”>POWER Data Access Viewer](https://power.nasa.gov/). The data are daily data, including rainfall (PRECIP), maximum temperature (T2M_MAX), minimum temperature (T2M_MIN), relative humidity (RH2M), wind speed (WS2M), and shortwave radiation (TOA_SW_DWN) data. In order to reflect the spatial climate variability throughout the watershed, the data were processed for 14 virtual station locations that were obtained from the CSIRO climate model (Figure 5). These data were formatted for SWAT input, enabling accurate simulation of climate-driven hydrological processes.

Model simulation and calibration

After delineating the watershed boundaries, establishing HRUs, and processing climate data,

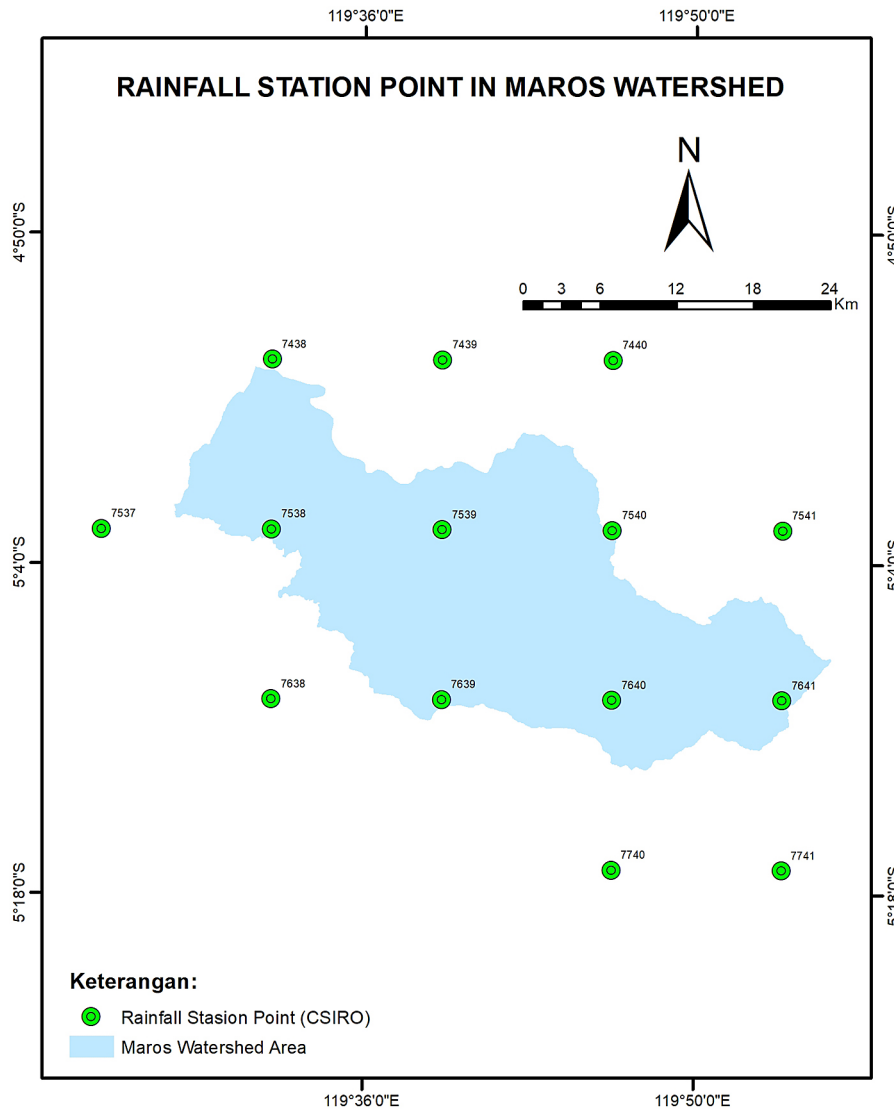


Figure 5. Rainfall station point of Maros watershed

we run the SWAT model simulation through the RUN SWAT menu. After the simulation process is complete, we can obtain SWAT output, one of which is the water yield. The SWAT model simulates water yield under two conditions, namely, existing conditions using the 2023 land cover map and projection conditions using the 2032 land cover projection map. The simulations were carried out after the model was previously calibrated and validated. To calibrate and validate the model, we use SWAT-CUP with an automatic optimization algorithm (SUFI-2). There are two rivers whose data are used as observation discharges, namely, the Batubassi and Lekopancing rivers, and river discharge data were obtained from the Pompengan Jeneberang River Basin. Furthermore, for calibration and validation, simulated and observed discharges are compared. The

results revealed that the coefficient of determination (R^2) for the Batubassi River was 0.7257 and that for the Lekopancing River was 0.7802. These values indicate adequate model performance on the basis of model evaluation criteria because the value of $R^2 > 0.6$ (Erraioui et al., 2023). To visually confirm the reliability of the model, scatter diagrams between observed and simulated discharge are shown in Figures 6 and 7.

Comparison of water yields in 2023 and projections for 2032

According to SWAT simulation. There are significant decline in water yield from 31.09 billion m^3 in 2023 to 21.65 billion m^3 in 2032, The water yield decreased by 9.44 billion m^3 (30.35%). The decline in rainfall (from 60.51 billion m^3 in

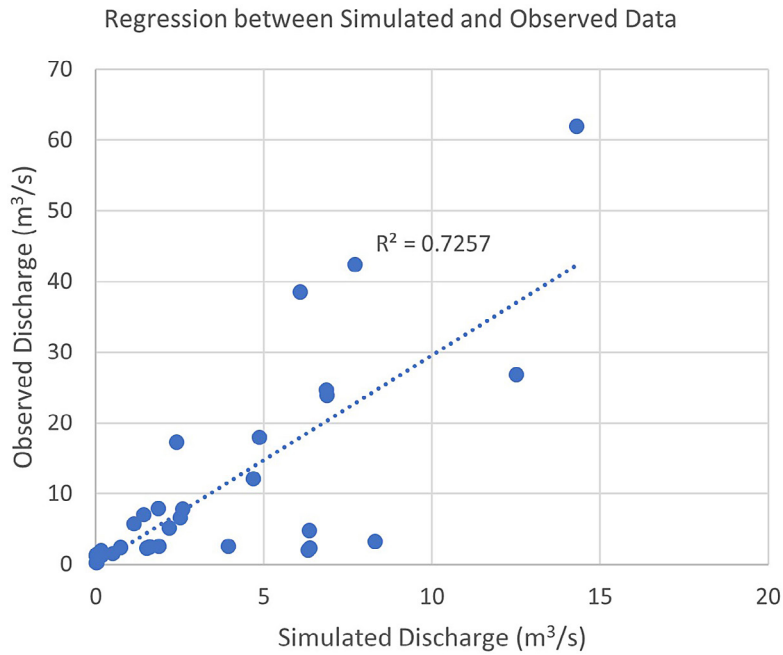


Figure 6. R^2 for Batubassi River

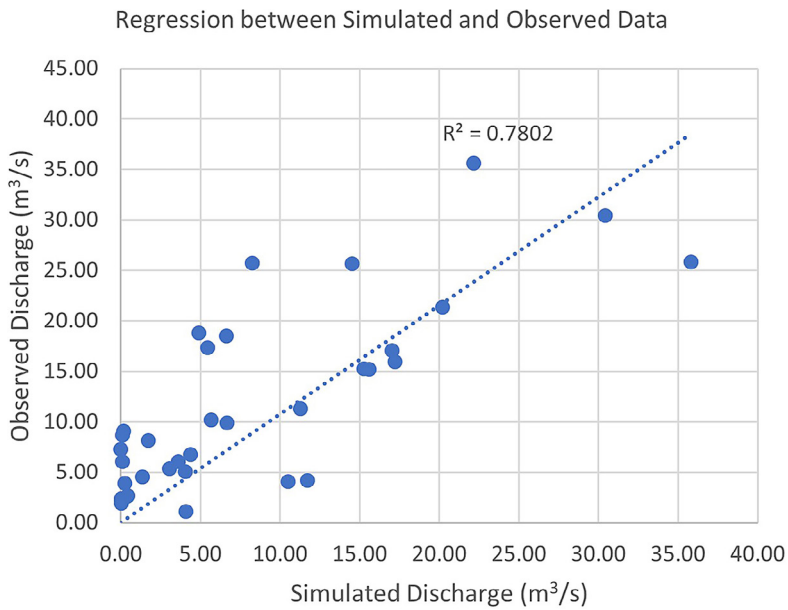


Figure 7. R^2 for Lekopancing River

2023 to 47.19 billion m^3 in 2032) and land cover changes are primarily responsible to this decline. Tables 5 and 6 show the components of monthly water yield, showing a decrease in surface runoff, lateral flow, and groundwater flow in 2032, reflecting changes in hydrological dynamics. In addition, ground flow can be negligible or zero, especially in dry months namely September, October, November, due to reduced infiltration and recharge, reflecting the impact of land cover changes and lower rainfall.

Impact of land cover changes on water yield

The dynamics of land cover change in the Maros watershed shows that the area of vegetated land cover is decreasing as it occurs in secondary forests and secondary mangrove forests. Secondary forests decreased in area from 25,223.95 hectares in 2023 to 25,015.40 hectares in 2032. Meanwhile, secondary mangrove forests decreased from 285.59 hectares in 2023 to 180.60 hectares in 2032. The decrease in vegetative land area is in

Table 5. Water yield of the Maros watershed in 2023 (in million m³)

Month	Precipitation (m ³)	Surface flow (m ³)	Lateral flow (m ³)	Ground flow (m ³)	WYLD (m ³)
1	11,929.23	2,458.69	3,125.46	296.08	5,880.23
2	17,118.98	5,558.09	3,610.87	1,174.78	10,343.73
3	4,633.82	388.21	887.94	2,050.66	3,326.81
4	5,722.71	886.67	1,364.91	1,368.92	3,620.50
5	2,400.65	326.67	448.00	746.97	1,521.64
6	3,284.69	246.93	501.10	202.79	950.82
7	3,660.65	816.07	862.06	169.32	1,847.44
8	51.82	0.0013	0.6826	75.89	76.57
9	63.26	0.0054	4.16	4.11	8.27
10	220.30	0.7650	10.75	0.0047	11.52
11	5,421.06	368.37	879.46	0.00001	1,247.82
12	6,000.76	798.72	1,423.70	37.87	2,260.28
Total	60,507.92	11,849.18	13,119.07	6,127.39	31,095.64

Table 6. Water yield of the Maros watershed in the projection year 2032 (in million m³)

Month	Precipitation (m ³)	Surface flow (m ³)	Lateral flow (m ³)	Ground flow (m ³)	WYLD (m ³)
1	16,582.02	4,419.78	4,436.86	319.16	9,175.81
2	7,542.78	1,209.38	1,663.10	1,241.67	4,114.16
3	3,795.99	305.40	692.84	1,329.55	2,327.79
4	3,896.34	739.83	790.37	678.75	2,208.95
5	2,623.27	48.37	479.99	238.55	766.91
6	1,582.33	29.73	261.55	69.33	360.60
7	241.71	0.3758	24.38	12.06	36.81
8	454.38	3.00	55.16	0.8328	58.99
9	9.26	0.1133	18.53	-	18.64
10	120.90	0.0067	1.34	-	1.35
11	2,928.10	39.52	350.33	-	389.86
12	7,414.27	431.67	1,762.32	0.5178	2,194.50
Total	47,191.34	7,227.18	10,536.76	3,890.42	21,654.35

line with the decline in the volume of water produced by the Maros watershed. This shows that the reduction in the area of secondary forests and mangrove forests that have an essential role in processes of hydrology including infiltration and groundwater recharge processes causes a reduction in the water yield in the Maros watershed.

Conversely, areas such as settlements, fish ponds, and paddy area have increased in size. settlements areas increased from 3,811.65 hectares in 2023 to 3,898.84 hectares in 2032. Fish ponds increased from 5,723.20 hectares in 2023 to 5,818.99 hectares in 2032. Paddy area increased from 14,007.22 hectares in 2023 to 14,093.81 hectares in 2032. The increase in the area of these lands is inversely proportional to the amount of

water produced in the watershed. This shows that the expansion in the area of land with impermeable characteristics such as settlements, fish ponds, and paddy area which generally increase surface runoff and reduce soil infiltration causes a reduction in the water yield produced in the Maros watershed.

These changes, combined with a 22% decrease in rainfall (from 60.51 to 47.19 billion m³), led to a 30.35% decrease in water yield. Figure 8 illustrates the spatial distribution of water yields, and shows a decline in water yields in areas where much forest has been lost and urban areas have expanded. Concerns about future water scarcity arise as the Maros watershed hydrological system faces increasing pressures as a result of the combined impacts of land cover change and climate.

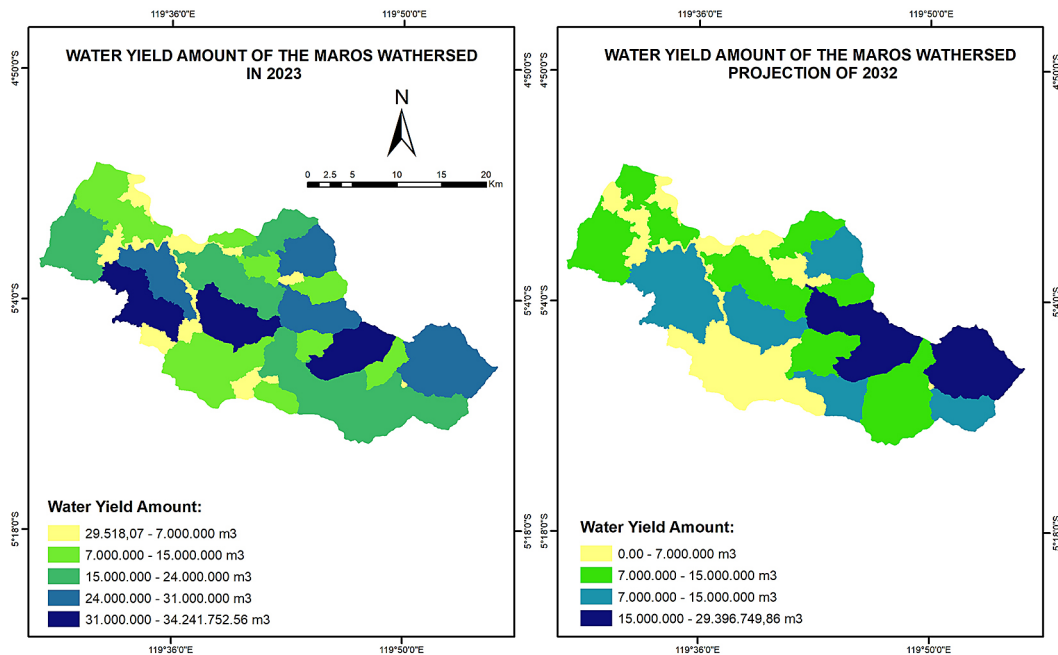


Figure 8. Map of the water yield in 2023 and 2032

CONCLUSIONS

The results of the 2032 land cover projection indicate that the land cover used for anthropogenic purposes, namely, settlements, fishponds, paddy areas, and agricultural/crop land, will increase in area, whereas vegetated land cover, namely, secondary forests and secondary mangrove forests, will decrease in area. These changes indicate that there has been development pressure on the natural ecosystems in the Maros watershed, which has affected the reduction in soil infiltration capacity, increased surface runoff, and reduced groundwater reserves, ultimately affecting the volume of water produced in the Maros watershed. The change in land cover from vegetation to land for anthropogenic purposes has caused a decline in the volume of water in the Maros watershed, as shown by the results of the SWAT model simulation, where there was a 30.35% decrease in water yield from 31.09 billion m³ in 2023 to 21.65 billion m³ in 2032. In addition to land cover changes, reduced rainfall also contributes to a decrease in water yield. These findings indicate that if these land cover changes are not controlled, the risk of drought, flooding, and seasonal water supply imbalances in the Maros watershed could increase.

Acknowledgments

Appreciation is conveyed to the Center for Development, Education, and Training of

Planners (Pusbindiklatren) Bappenas for funding this research and the Regional Development Planning Study Program of Hasanuddin University for granting permission to conduct this research. This research is part of a thesis submitted as one of the academic requirements.

REFERENCES

1. Abbas, Z., Yang, G., Zhong, Y., Zhao, Y. (2021). Spatiotemporal change analysis and future scenario of lulc using the CA-ANN approach: A case study of the greater bay area, China. *Land*, 10(6). <https://doi.org/10.3390/land10060584>
2. Amgoth, A., Rani, H. P., Jayakumar, K. V. (2023). Exploring LULC changes in Pakhal Lake area, Telangana, India using QGIS MOLUSCE plugin. *Spatial Information Research*, 31(4). <https://doi.org/10.1007/s41324-023-00509-1>
3. Amin, N., Lias, S. A., Ahmad, A. (2021). Potential landslide-prone areas in the Kelara sub-watershed using the analytical hierarchy process method. *IOP Conference Series: Earth and Environmental Science*, 807(2). <https://doi.org/10.1088/1755-1315/807/2/022080>
4. Anggari, E. A., Herawan, A., Hakim, P. R., Wahyudiono, A., Salaswati, S., Rachim, E., Zyslhal, Z. (2023). Assessing the Accuracy of Land Use Classification Using Multi-spectral Camera From LAPAN-A3, Landsat-8 and Sentinel-2 Satellite: A Case Study in Probolinggo-East Java. *International Journal on Advanced Science, Engineering*

- and Information Technology, 13(5). <https://doi.org/10.18517/ijaseit.13.5.18570>
5. Aznarez, C., Jimeno-Sáez, P., López-Ballesteros, A., Pacheco, J. P., Senent-Aparicio, J. (2021). Analysing the impact of climate change on hydrological ecosystem services in laguna del sauce (Uruguay) using the swat model and remote sensing data. *Remote Sensing*, 13(10). <https://doi.org/10.3390/rs13102014>
 6. Badwi, N., Yusuf, M., Anam, M. C. (2023). Deforestation profile in the Maros Watershed, South Sulawesi Province. *LaGeografia*, 21(2), 194–208. <https://ojs.unm.ac.id/Lageografia/article/view/43243/pdf>
 7. Barkey, R. A., Nursaputra, M. (2019). The Detection of Forest Health Level as an Effort to Protecting Main Ecosystem in the term of Watershed Management in Maros Watershed, South Sulawesi. *IOP Conference Series: Earth and Environmental Science*, 270(1). <https://doi.org/10.1088/1755-1315/270/1/012006>
 8. Busico, G., Colombani, N., Fronzi, D., Pellegrini, M., Tazioli, A., Mastrocicco, M. (2020). Evaluating SWAT model performance, considering different soils data input, to quantify actual and future runoff susceptibility in a highly urbanized basin. *Journal of Environmental Management*, 266. <https://doi.org/10.1016/j.jenvman.2020.110625>
 9. Dahal, P., Shrestha, M. L., Panthi, J., Pradhananga, D. (2020). Modeling the future impacts of climate change on water availability in the Karnali River Basin of Nepal Himalaya. *Environmental Research*, 185. <https://doi.org/10.1016/j.envres.2020.109430>
 10. Dutra, D. J., Elmiro, M. A. T., Ribeiro, S. M. C. (2022). Association between forest resources and water availability: temporal analysis of the Serra Azul stream sub-basin. *Anais da Academia Brasileira de Ciências*, 94(3). <https://doi.org/10.1590/0001-376520220201289>
 11. Enderwin, E., Kasih, B. T. H., Gunawan, D. (2013). Determination of threshold values for the variability index (VI) and optimal rainfall intensity for estimating rainfall in indonesia using a modified convective stratiform technique (CSTm). *Jurnal Meteorologi dan Geofisika*, 14(1). <https://doi.org/10.31172/jmg.v14i1.141>
 12. Erraioui, L., Taia, S., Taj-Eddine, K., Chao, J., El Mansouri, B. (2023). Hydrological modelling in the ouerga watershed by soil and water analysis tool. *Journal of Ecological Engineering*, 24(4). <https://doi.org/10.12911/22998993/161043>
 13. Femeena, P. V., Karki, R., Cibir, R., Sudheer, K. P. (2022). Reconceptualizing HRU Threshold definition in the soil and water assessment tool. *Journal of the American Water Resources Association*, 58(4). <https://doi.org/10.1111/1752-1688.13000>
 14. Imran, A. N., Djafar, M. (2020). The Influence of ecosystem knowledge, conservation knowledge, and pollution knowledge on community environmental stewardship attitudes in the upper maros Watershed Area, Maros Regency. *Jurnal Eboni*, 2(1), 1–11. <https://ejournals.umma.ac.id/index.php/eboni/article/view/610/465>
 15. Islam, K., Daraio, J., Sabau, G., Cheema, M., Galagedara, L. (2024). Insights to the water balance of a Boreal watershed using a SWAT model. *Environmental Research Communications*, 6(5). <https://doi.org/10.1088/2515-7620/ad495c>
 16. Latief, R., Barkey, R. A., Suhaeb, M. I. (2021). Land use change and flooding in the Maros River Basin. *Urban and Regional Studies Journal*, 3(2). <https://doi.org/10.35965/ursj.v3i2.669>
 17. Lukas, P., Melesse, A. M., Kenea, T. T. (2023). Prediction of future land use/land cover changes using a coupled CA-ANN model in the upper Omo–Gibe River Basin, Ethiopia. *Remote Sensing*, 15(4). <https://doi.org/10.3390/rs15041148>
 18. Muhammad, R., Zhang, W., Abbas, Z., Guo, F., Gwi-azdzinski, L. (2022). Spatiotemporal change analysis and prediction of future land use and land cover changes using QGIS MOLUSCE plugin and remote sensing big data: a case study of Linyi, China. *Land*, 11(3). <https://doi.org/10.3390/land11030419>
 19. Neitsch, S., Arnold, J., Kiniry, J., Williams, J. (2011). Soil & Water Assessment Tool Theoretical Documentation Version 2009. *Texas Water Resources Institute*, 1–647. <https://doi.org/10.1016/j.scitotenv.2015.11.063>
 20. Nurhidayat. (2022). *Effect of Land Cover Changes on River Flow Components in Sub Tanralili*. Thesis. Faculty of Agriculture, Hasanuddin University: Makassar
 21. Nurmiaty, Baja, S. (2013). Assessing land use dynamics using GIS-based Cellular Automata and Markov Chain. *34th Asian Conference on Remote Sensing 2013, ACRS 2013*, 5(4), 4062–4068.
 22. Pahar, S. P. P., Paembonan, S. A., Soma, A. S. (2021). Identification of drought level using normalized difference latent heat index on Maros Watershed. *IOP Conference Series: Earth and Environmental Science*, 681(1). <https://doi.org/10.1088/1755-1315/681/1/012123>
 23. Ridwansyah, I., Fakhrudin, M., Wibowo, H., Yulianti, M. (2018). Application of the soil and water assessment tool (SWAT) to predict the impact of best management practices in Jatigede Catchment Area. *IOP Conference Series: Earth and Environmental Science*, 118(1). <https://doi.org/10.1088/1755-1315/118/1/012030>
 24. Sari, Tri Linda. (2022). *Erosion Hazard Level Analysis Using the SWAT Model (Soil and Water Assessment Tool) in Tanralili Sub-watershed*. Thesis. Faculty of Agriculture, Hasanuddin University: Makassar
 25. Smit, E., van Zijl, G., Riddell, E., van Tol, J. (2024). Model calibration using hydro-pedological insights to improve the simulation of internal hydrological

- processes using SWAT+. *Hydrological Processes*, 38(5), 1–16. <https://doi.org/10.1002/hyp.15158>
26. Syafri, S., Surya, B., Ridwan, R., Bahri, S., Rasyidi, E. S., Sudarman, S. (2020). Water quality pollution control and watershed management based on community participation in maros city, south sulawesi, indonesia. *Sustainability (Switzerland)*, 12(24). <https://doi.org/10.3390/su122410260>
 27. Thakur, J. K., Khanal, K., Poudyal, K. (2017). Assessment of regional changes for enhancing water availability. *Environmental Systems Research*, 6(1). <https://doi.org/10.1186/s40068-017-0096-3>
 28. Tian, Y., Xu, D., Song, J., Guo, J., You, X., Jiang, Y. (2022). Impacts of land use changes on ecosystem services at different elevations in an ecological function area, northern China. *Ecological Indicators*, 140. <https://doi.org/10.1016/j.ecolind.2022.109003>
 29. Tran, T. N. D., Nguyen, B. Q., Vo, N. D., Le, M. H., Nguyen, Q. D., Lakshmi, V., Bolten, J. D. (2023). Quantification of global digital elevation model (DEM) – A case study of the newly released NA-SADEM for a river basin in Central Vietnam. *Journal of Hydrology: Regional Studies*, 45. <https://doi.org/10.1016/j.ejrh.2022.101282>
 30. Truong, N. C. Q., Khoi, D. N., Nguyen, H. Q., Kondoh, A. (2022). Impact of forest conversion to agriculture on hydrologic regime in the large Basin in Vietnam. *Water (Switzerland)*, 14(6). <https://doi.org/10.3390/w14060854>
 31. Wiwoho, B. S., Astuti, I. S., Alfarizi, I. A. G., Sucahyo, H. R. (2021). Validation of three daily satellite rainfall products in a humid tropic watershed, brantas, indonesia: Implications to land characteristics and hydrological modelling. *Hydrology*, 8(4). <https://doi.org/10.3390/hydrology8040154>
 32. Zare, M., Azam, S., Sauchyn, D. (2022). Evaluation of soil water content using SWAT for Southern Saskatchewan, Canada. *Water (Switzerland)*, 14(2). <https://doi.org/10.3390/w14020249>